

Spatial mechanical behaviors of long-span V-shape rigid frame composite arch bridges

Hongye Gou^{*1}, Qianhui Pu^{1a}, Junming Wang^{2b}, Zeyu Chen^{3c} and Shiqiang Qin^{1d}

¹Department of Bridge Engineering, Southwest Jiaotong University, Chengdu, 610031, P.R. China

²Architecture and Survey Design Institute of Southwest Jiaotong University, Chengdu, 610031, P.R. China

³China Railway Siyuan Survey and Design Group Co. Ltd., Wuhan, 430063, P.R. China

(Received July 9, 2012, Revised May 7, 2013, Accepted July 3, 2013)

Abstract. The Xiaolan channel super large bridge is unique in style and with greatest span in the world with a total length of 7686.57 m. The main bridge with spans arranged as 100m+220m+100m is a combined structure composed of prestressed concrete V-shape rigid frame and concrete-filled steel tubular flexible arch. First of all, the author compiles APDL command flow program by using the unit birth-death technique and establishes simulation calculation model in the whole construction process. The creep characteristics of concrete are also taken into account. The force ratio of the suspender, arch and beam is discussed. The authors conduct studies on the three-plate webs's rule of shear stress distribution, the box girder's longitudinal bending normal stress on every construction stage, meanwhile the distribution law of longitudinal bending normal stress and transverse bending normal stress of completed bridge's box girder. Results show that, as a new combined bridge, it is featured by: Girder and arch resist forces together; Moment effects of the structure are mainly presented as compressed arch and tensioned girder; The bridge type brings the girder and arch on resisting forces into full play; Great in vertical stiffness and slender in appearance.

Keywords: bridge engineering; long-span V-shape rigid frame composite arch bridge; simulation calculation in the whole construction process; stress distribution law; spatial mechanical behaviors

1. Introduction

Long-span V-shape rigid frame composite arch bridge is a composite structure system which uses V-shape rigid frame as the main part and arch as the supplement to bear stress. With a combination of V-shape rigid frame's extended shape, arch's smooth shape and thrust balance, the advantage of V-shape rigid frame can be promoted at full play. It has good mechanical properties, reasonable technical and economic index and abundant landscape effect (Nakamura *et al.* 2009, Tao 2011, Roeder *et al.* 2000).

*Corresponding author, Associate Professor, E-mail: gouhongye@163.com

^aProfessor, E-mail: qhpu@vip.163.com

^bM.C.E. Engineer, E-mail: 116613097@qq.com

^cM.C.E. Engineer, E-mail: 83982871@qq.com

^dPh.D. Student, E-mail: 394013589@qq.com

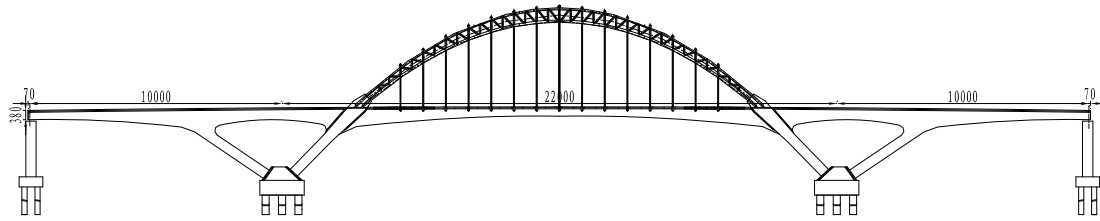


Fig. 1 Elevation of the Xiaolan channel super large bridge (unit: cm)

With the increase of the modern composite bridge' span, bridge's horizontal width is getting larger. The spatial effect of long-span V-shape rigid frame composite arch bridge is increasingly obvious as well. Therefore, the result of plane analysis cannot reflect the bridge's real force conditions properly (Ma 2011, Haensel 1998, Ribeiro 2012).

Long-span V-shape rigid frame composite arch bridge is a beam-arch combination system in which the main girder is continuous and piers are consolidated with the girder. Three-direction prestressed system is usually adopted in this kind of bridge, hence the force conditions are complex and the spatial effects are also evident. Nevertheless, it is impossible to calculate the stress conditions of V-Shape Piers. For the safety of bridge structure, it is necessary to do spatial behavior analysis (Altunisik *et al.* 2010, Pan 2011, Chen 2002) for the whole structure.

The Xiaolan channel super large bridge is part of Guangzhou-Zhuhai intercity rapid rail transit project bid section ZH-1. It is the first time that this kind of bridge has been adopted in domestic passenger dedicated railway line. It is unique in style and with greatest span in the world with a total length of 7686.57 m. The main bridge with spans arranged as 100m+220m+100m is a combined structure composed of prestressed concrete V-shape rigid frame and concrete-filled steel tubular flexible arch. Prestressed concrete continuous rigid frame and concrete-filled steel tube arch bridge take load together in this structure, furthermore the structural internal force is influenced by the rigidity, temperature, shrinkage and creep in every part. Therefore, the stress, bearing force and transmission force in the structure is complex (Gou *et al.* 2010) The elevation drawing of Xiaolan super large bridge is shown in Fig. 1.

2. Simulation calculation of the whole construction process

2.1 Construction scheme

Prestressed concrete V-shape rigid frame composite concrete-filled steel tube arch structure is adopted in the Xiaolan channel super large bridge. As a rigid beam-flexible arch system, the arch rib is flexible, therefore, the prior consideration of the system stability during the construction is necessary. On the basis of comparison and analysis of stresses, "Erection of the continuous girder prior to that of the arches" is adopted as the construction scheme, the construction of the arch should be done after the closure of the continuous rigid frame and the formation of stable system. In this construction plan, brackets and steel arch rib rotation tower trusses are installed on the surface of continuous rigid frame, then install the steel arch ribs with vertical rotation method. The installation of arch ribs, vertical rotation and suspender tension are all arranged after the closure of the main girder.

2.2 Element birth and death

In finite element analysis, adding or deleting materials in the model means birth or death of the corresponding elements. Element birth and death technology is applied under this condition. The mathematical equations below are used to expound the principle of Element birth and death (Wang 2012, Roberts 2009, Lee 2009).

In finite element analysis, nodal force $\{f_i^e\}$ and node displacement $\{s_i^e\}$ in any element i have the relationship below

$$\{f_i^e\} = [k_i^e] \{s_i^e\} \quad (1)$$

Where $[k_i^e]$ is element stiffness matrix, subscript i is the number of the element.

If structural finite element model has n elements, there are n relations between forces and displacements as the forms below

$$\begin{Bmatrix} \{f_1^e\} \\ \{f_2^e\} \\ \vdots \\ M \\ \vdots \\ \{f_n^e\} \end{Bmatrix} = \begin{bmatrix} [k_1^e] & & & & \\ & [k_2^e] & & & \\ & & 0 & & \\ & & & [k_i^e] & \\ & & & & 0 \\ & & & & & [k_n^e] \end{bmatrix} \begin{Bmatrix} \{s_1^e\} \\ \{s_2^e\} \\ \vdots \\ M \\ \vdots \\ \{s_n^e\} \end{Bmatrix}$$

$$\text{Namely} \quad \{f\} = [k] \{s\} \quad (2)$$

Transfer to structural finite element equilibrium equation with displacement transformation matrix $[A]$

$$[K] \{\delta\} = \{P\} \quad (3)$$

Where $[K]$ is combined global stiffness matrix, $[K] = [A]^T [K] [A]$; $\{\delta\}$ is structure displacement vector, $\{\delta\} = [A]^{-1} \{s\}$; $\{P\}$ is nodal load vector, $\{P\} = [A]^T \{f\}$.

Formula (2) can be local modified by multiplying stiffness matrix $[k_i^e]$ by stiffness factor λ_i , λ_i is used to control the property of elements "birth and death". The modified formula of the relation between nodal force and node displacement is

$$\{f_i^e\} = \lambda_i [k_i^e] \{s_i^e\} \quad (4)$$

Non-combined stiffness matrix composed of all structure elements is

$$[k] = \begin{bmatrix} \lambda_1 [k_1^e] & & & & \\ & \lambda_2 [k_2^e] & & & \\ & & 0 & & \\ & & & \lambda_i [k_i^e] & \\ & & & & 0 \\ & & & & & \lambda_n [k_n^e] \end{bmatrix} \quad (5)$$

Therefore, it is easy to control the birth and death of each element by using λ_i . If element i is defined to be dead, the value λ_i is adopted zero instead of removing the dead element. Meanwhile, add parameters related with this dead element such as element load (concentrated force, uniform force, initial stress, temperature load, etc.), weight, damping, specific heat and other properties to the model. It is convenient to activate the load and other properties of any element by valuing $\lambda_i = 1$.

2.3 Calculation of concrete shrinkage and creep

Creep coefficient φ should be determined before creep calculation. Creep model is an arithmetic based on relative parameters to predict φ . Numerous creep models are adopted by foreign countries, ACI, CEB-FIP, BP are commonly used.

The type of creep model is mainly determined by practical accuracy, which is an important and complicated problem. Numerous types of models are adopted by foreign codes; CEB-FIP1990 is promulgated, but current China Railway Bridge code (TB10002.1-2005 2005) still uses CEB-FIP1978 model. In this model, load age is τ , calculation age is t , the creep coefficient of concrete is

$$\varphi(t, \tau) = \beta_a(\tau) + 0.4\beta_d(t - \tau) + \varphi_f[\beta_f(t) - \beta_f(\tau)] \quad (6)$$

In China Railway Bridge code, the computing pattern of creep coefficient is in the form of graph curves and tables, therefore, it is inconvenient for zooming but is featured by high precision. If the curves A.0.2-1~A.0.2-4 are magnified and converted to discrete data sheets, the calculation will be convenient and accurate. It is necessary to transform formula (6) to a proper formula for zooming:

Non-recovered plastic deformation at initial loading stage

$$\beta_a(\tau) = 0.8(1 - \frac{f_\tau}{f_\infty}) = 0.8 \times [1 - \frac{1}{1.276} (\frac{\tau}{4.2 + 0.85\tau})^{3/2}] \quad (7)$$

Lagging elastic strain increased with time

$$\beta_d(t - \tau) = 0.73 \times [1 - e^{-0.01(t - \tau)}] + 0.27 \quad (8)$$

Lagging plastic strain increased with concrete ages

$$\varphi_f[\beta_f(t) - \beta_f(\tau)] = \varphi_{f1}\varphi_{f2} [(\frac{t}{t + H_f})^{1/3} - (\frac{\tau}{\tau + H_f})^{1/3}] \quad (9)$$

Where $\varphi_f = \varphi_{f1}\varphi_{f2}$ is flow plastic coefficient, φ_{f1} is the coefficient determined by environment, φ_{f2} is the coefficient determined by theoretical thickness; $\beta_f(t)$ and $\beta_f(\tau)$ are lagging plastic strain with the increase of concrete ages, they are related with the theoretical thickness.

Calculate out creep coefficient $\varphi(t, \tau)$ in formula (6), and then work out creep strain, finally conduct simulation solution by imposing temperature.

2.4 Study on the simulation of prestressing effect in bridge spatial analysis

Three methods are commonly used in simulation of prestressing effect: imposing element's

initial strain, imposing element's temperature variation and equivalent load by taking the temperature into account. Former two methods are of separate type modeling. In these methods, concrete and reinforcement are modeled separately, and the nodes must be coincident to ensure that the prestressing effect can transmit to the concrete structure. Furthermore, the third one is a regular method.

Solid elements are used in the model of Xiaolan channel super large bridge. Traditional method of dividing elements consumes plenty of time and energy, therefore, the theory of separate model for coupled method based on the analysis of finite element model is adopted. The basic idea is building solid elements model and tendon model separately without considering the relationship between them, then dividing the elements of each model separately and connecting solid element with tendon element at the node with coupling equation. This method is simple with less time. The simulation of prestressing effect can be realized by decreasing the temperature on the tendon.

2.5 Simulation calculation model of whole construction process

ANSYS element's birth and death technology is used in the simulation calculation of the construction of Xiaolan channel super large bridge. In the calculation, APDL command flow program is compiled and concrete's creep property is under consideration. In the study of the stage construction of "Erection of the continuous girder prior to that of the arches", simulation calculation model of the whole construction process is established.

In the simulation analysis of prestressed concrete V-shape rigid frame and concrete-filled steel tubular flexible arch composite bridge, four element types of ANSYS are used.

(1) Spatial solid element (SOLID45): simulated girder, inclined legs, pile cap and pile foundation;

(2) Spatial beam element (BEAM44): simulated arch rib and tie cable;

(3) Cable element: simulated prestressing tendon and suspender;

(4) 3-D structure surface effect unit (SURF154) : Used in live loads and surface effects, can be covered on the surface of any 3D element, simulated construction temporary load, secondary permanent load, etc.

The connection between solid element and beam element or cable element uses dof coupling, namely the rigid joint.

In pre-treatment, the four types of elements above are adopted in whole bridge finite element model, where are 263133 nodes and 1126921 elements (1035183 SOLID45 elements, 998 BEAM44 elements, 12554 LINK8 elements, 78186 SURF154 elements). In coordinate system, Z for bridge longitudinal direction, X for horizontal direction, Y for vertical direction. The discretization figures of whole bridge finite element model are shown in Fig. 2.

3. Stress ratio analysis of suspender, arch and girder

3.1 Stress ratio of the suspender

As shown in Fig. 3, vertical uniform load $q = 160$ kN/m is imposed on bridge deck, the deformation of the main girder, suspender and arch rib is due to vertical load exerted on main girder directly. And the load is distributed according to stiffness on the basis of deformation compatibility. Under this uniform load, the tensile forces of rod which are close to mid span

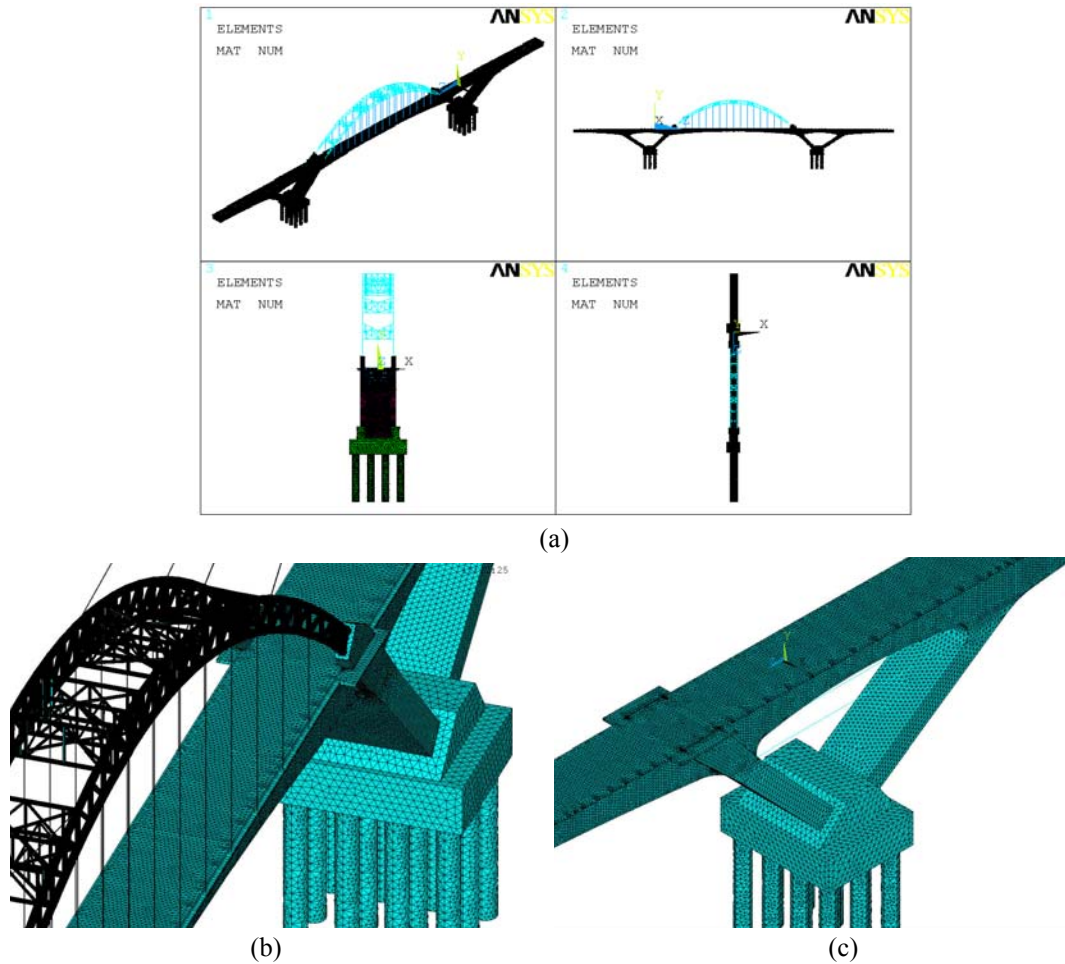


Fig. 2 Discretization figures of finite element model of the Xiaolan channel super large bridge

increase greater than those which are close to skewback. The proportion of the total vertical load ($q \times 220$) accounted by the increment of all suspenders of main span is ($\eta_1 = 60.99\%$).

3.2 Ratio of the forces in arch rib section and girder section

Under the vertical load $q = 160$ kN/m, the force condition of girder and arch rib sections are shown as Fig. 4, the bending moment of arch rib $M_A = 7334$ kN.m, axial force $H_A = 7391$ kN; and the bending moment of main girder $M_G = 42040$ kN.m.

The total effect moment of the mid span section of the whole structure is: $M_i^0 = 42040 + 7334 + 7391 \times 37.287 = 324962$ (kN.m).

The moment distribution coefficient of crown section is: $u_i^a = 7334 / (7334 + 42040) \times 100\% = 14.85\%$.

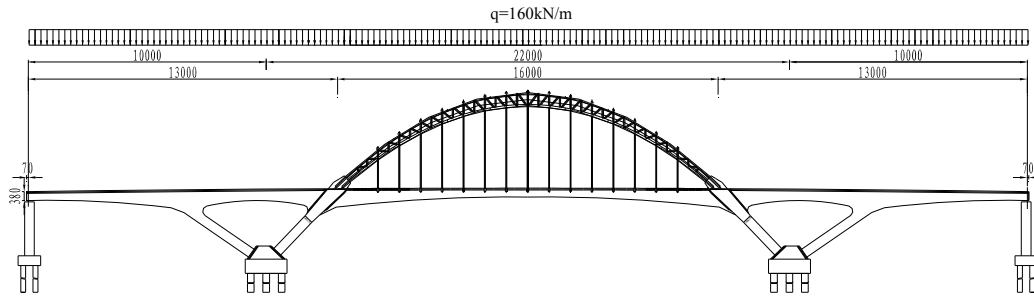


Fig. 3 Deck loading diagram of force comparison of the suspender, arch and beam(unit: cm)

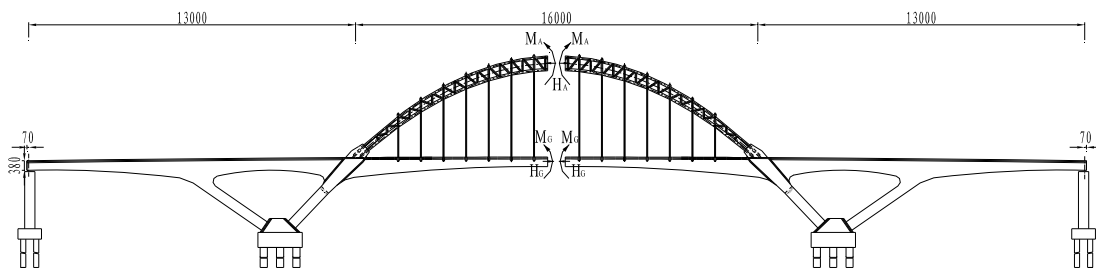


Fig. 4 Internal force diagram under longitudinal uniform distribution load(unit: cm)

The moment distribution coefficient of main girder's mid span section is: $u_i^b = 42040 / (7334 + 42040) \times 100\% = 85.15\%$.

From the results above, it is clear that under the vertical uniform load, the total moment above the mid span section of the structure M_i^0 is converted to the stress in the arch rib and the tension in the main girder which shows the superiority of beam arch combination structure. The bending moment in the girder is much greater than that in the arch rib, because the arch is relative flexible.

4. Rule of shear stress distribution in three webs

The cracks always appear in completed bridges, especially after secondary dead loads being imposed, thus the focuses of spatial analysis of box girder are on the stress and behavior under the dead loads and prestress in the last construction phase. The main dead load with a value of 26kN/m^3 is main girder's structural dead weight at vertical downwards side. Secondary dead loads (bridge deck pavement, etc.), use surface distribution loads to imitate the effect produced by bridge deck pavement (including green belts, etc.) on the structure whose value is 13.793kN/m^2 at vertical downwards side. The cable force in every suspender reaches the completed bridge design cable force. Use 3-D model to calculate the forces condition in the completed bridge and conclude the mechanical law of this structure to work out the contribution law of shearing stress in these three main girders' webs and the box girders' transverse force characteristics.

The webs are mainly designed to bear shearing force, thus the webs' force contribution is actually the shearing stress distribution under loads. The trend chart of the shearing force in the

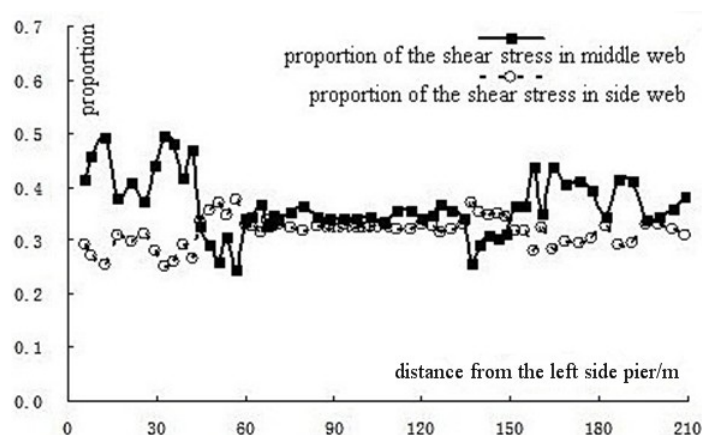


Fig. 5 Web shear stress distribution trend diagram in each section of axial direction bridge

webs of every section in bridge's axial direction is shown in Fig. 5.

Because the construction process is not imitated and the arch effects in the structure's force distribution are over improved, the results of shearing forces in the girder sections closed to piers' top are relatively small under circumstances that general spatial simulative analysis cannot consider the construction process. In element birth and death nonlinear simulation analysis, the whole construction process is under consideration, the results of shearing force are exact. In Fig. 5, the distribution of shearing force in every section is in continuous variation with better regularity. The forces in the webs of both sides are accordant, except for the sections on the left of element C0-1 (Fig. 5, 44.95-56.95m on horizontal ordinate) and on the right of element C0-2 (Fig. 5, 136.5-148.5m on horizontal ordinate). In these sections, the forces on edge webs are larger than those on middle webs, but in other sections, the forces on middle webs are larger. The shearing force ratio of middle and edge webs in the sections of side span is relatively larger, which is about 1.20~1.96; and the ratio in the sections of main span is about 1.03~1.55; The element 0 and these three webs of the box girder on the top of the V-shape pier are stressed uniformly in accordance with structure forces.

5. Spatial stress analysis of box girder

5.1 Longitudinal bending positive stress of box girder at each construction stage

Extract maximum compressive stress and maximum tensile stress in each section at every construction stage, and draw construction stress envelope diagram (Fig. 6). In the quantitative value “-” stands for pressure stress and “+” stands for tensile stress. The graph shows that the construction envelope stress of the main girder is -18.60MPa~1.73MPa. The maximum tensile stress appears in element 0 on the top of V-shape pier, on the bottom plate of element C3's right box girder when closure block C5 on the top of V-shape pier is being poured and prestressed reinforcement is not being tensioned. The maximum compressive stress appears on the top plate of element B10's left box girder in side span when mid span closure block A21 is being poured and prestressed reinforcement is not being tensioned. As a whole, longitudinal positive stress of each

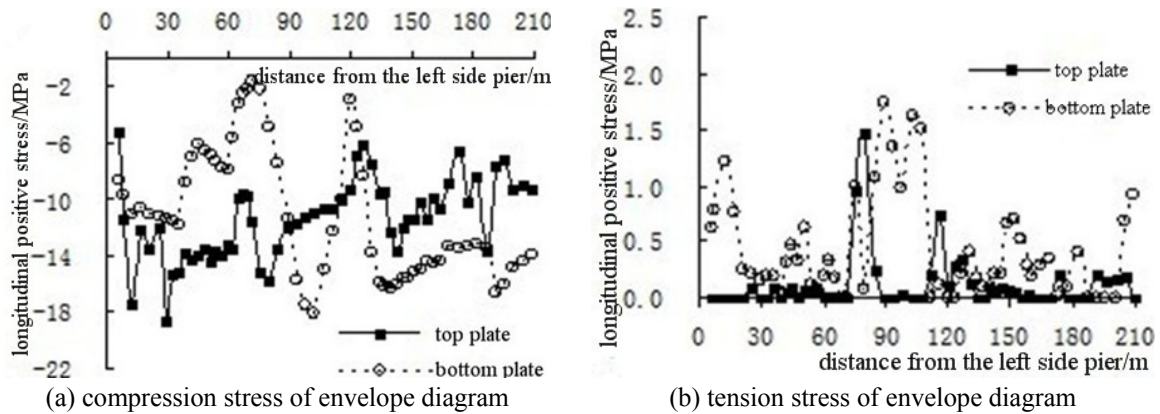


Fig. 6 Envelope diagram of maximum tension-compression stress of main girder in construction stages

section at construction stage can meet standard requirements (permissible value of construction compressive stress is -40.00MPa , and permissible value of construction tensile stress is 3.50MPa), which indicates that longitudinal prestress can make the whole bridge in pressured state in longitudinal direction, and the expected purpose is achieved.

As a variable cross-section box girder bridge, stage construction method is adopted; the elements are poured by sections from V-shape pier beam trigonometry area to both sides. In the construction period, the bending moment caused by constant load and prestress will impose effect on cantilever part and lead to enormous effects in the element 0's box girder on the top of V-shape pier. At the same time, the stress state of element 0 is related to the state of the whole structure.

The authors carry construction monitoring and control of V-shape rigid frame composite arch bridge, thus the measured values of longitudinal bending positive stress are obtained in order to give real time safety pre-warning when beyond limitation and to ensure the safety of the structure. There are 28 stress test sections in total in this bridge. The total stress measuring points are 128 in main girder and inclined leg sections, 32 in arch rib steel tube surface, and 12 in inner inclined leg joint sections located in the middle web. The whole stress measuring points of the bridge are 172. Select the average test value of measuring points at key sections for analysis. The graphs below (Figs. 7~8) list the contrast results of measured value and calculated value of the longitudinal bending positive stress in top and bottom plate of B-B and D-D (Fig. 9) sections of element 0's root on the top of V-shape pier.

The contrast results of measured value and calculated value of construction stress at each stage indicate:

(1) At each construction stage, the stress state growing trend of section B-B and D-D's top and bottom plate of element 0 on the top of V-shape pier is in accordance with calculated results and the measured value basically tallied with the theoretical value, in which the biggest difference is 1.83MPa .

(2) Tensile stress almost does not appear in the construction process, but in uniform variation and without mutation, which indicates that the structure loading of element 0's box girder is reasonable. The stress value of each measuring point is within standard permissible value, indicating that this bridge is safe in the construction process of erection of the continuous girder prior to that of the arches.

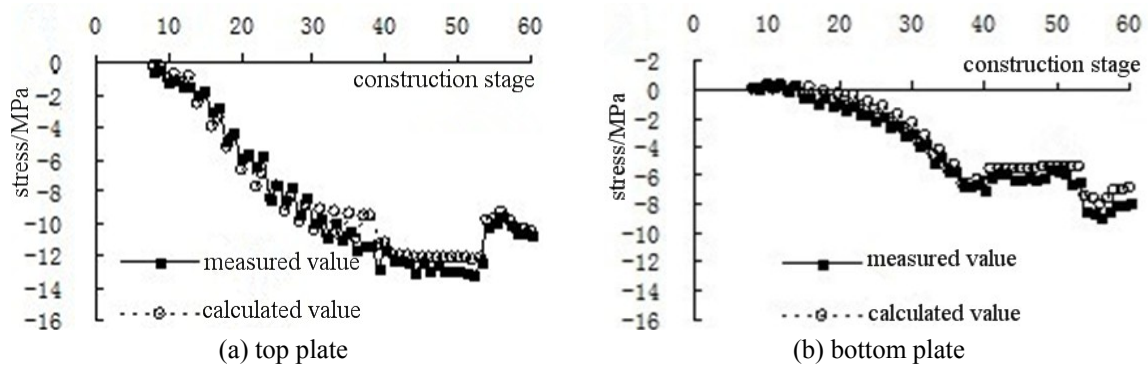


Fig. 7 Comparison results of stress measured values and calculated values in section B-B

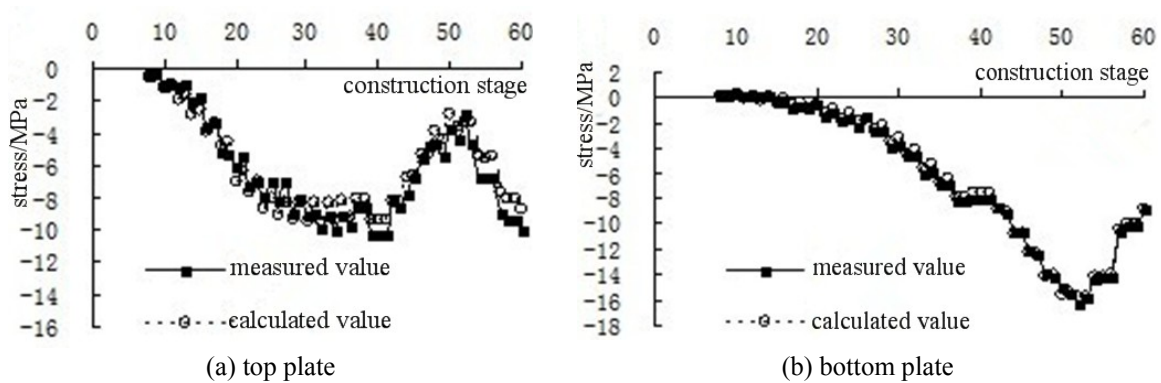


Fig. 8 Comparison results of stress measured values and calculated values in section D-D

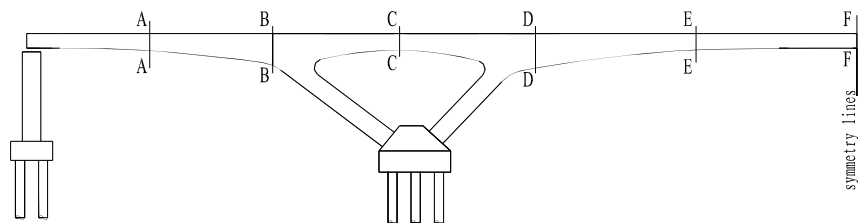


Fig. 9 Schematic diagram of calculation section in half-bridge structure

5.2 Longitudinal bending positive stress of completed bridge's box girder

This bridge is a variable cross-section single box double room bridge, whose shear lag effect has some effects on the positive stress of top and bottom plate. Thus stage construction method is adopted; the elements are poured by sections from beam's shoulder to both sides. During the construction period, the negative bending moment caused by constant load and prestress will impose effect on cantilever part and lead to enormous shear lag effect in the beam.

After system transformation, under dead loads, the force condition of this kind of bridge is close to that of cantilever beam. However, the beam section's stress variation caused by shear lag

effect cannot be ignored. Select six typical sections to analyze the stress variation of box girder's top and bottom plate under dead weight and prestress in the late completed bridge period. These six sections are A-A (the mid-span section of bridge's side span); B-B (the junction section of V-shape pier and girder of the side span); C-C (the section at the center of V-shape pier's top); D-D (the junction section of V-shape pier and girder of the mid span); E-E (the section at the 1/4 of mid span); F-F (mid-span section of mid span). The schematic diagram of the half bridge structure's calculation section is shown in Fig. 9. The transversal distribution of each section's longitudinal bending positive stress is shown in Fig. 10.

The graph shows that the transversal distribution of longitudinal bending positive stress in section A-A, B-B, D-D and E-E's top plate is obviously uneven. Different from the predicted value given by elementary beam theory, the spatial effect and shear lag effect of prestress are obvious. But the shear lag effect of longitudinal bending positive stress in the section at the center of V-shape pier's top and mid-span of the mid span, the bottom plate of each section as well, is not very obvious, which is similar to the predicted value given by elementary beam theory.

The stress in the joint of flange and web is larger than that in the center at the sections of A-A and E-E, which is called positive shear lag phenomenon. And negative shear lag phenomenon appears at section B-B and D-D, because these sections are near cross strut at negative moment area. The restriction effect of pier and girder's consolidation point makes shear transfer from the junction of web and flange to plate's center lagged.

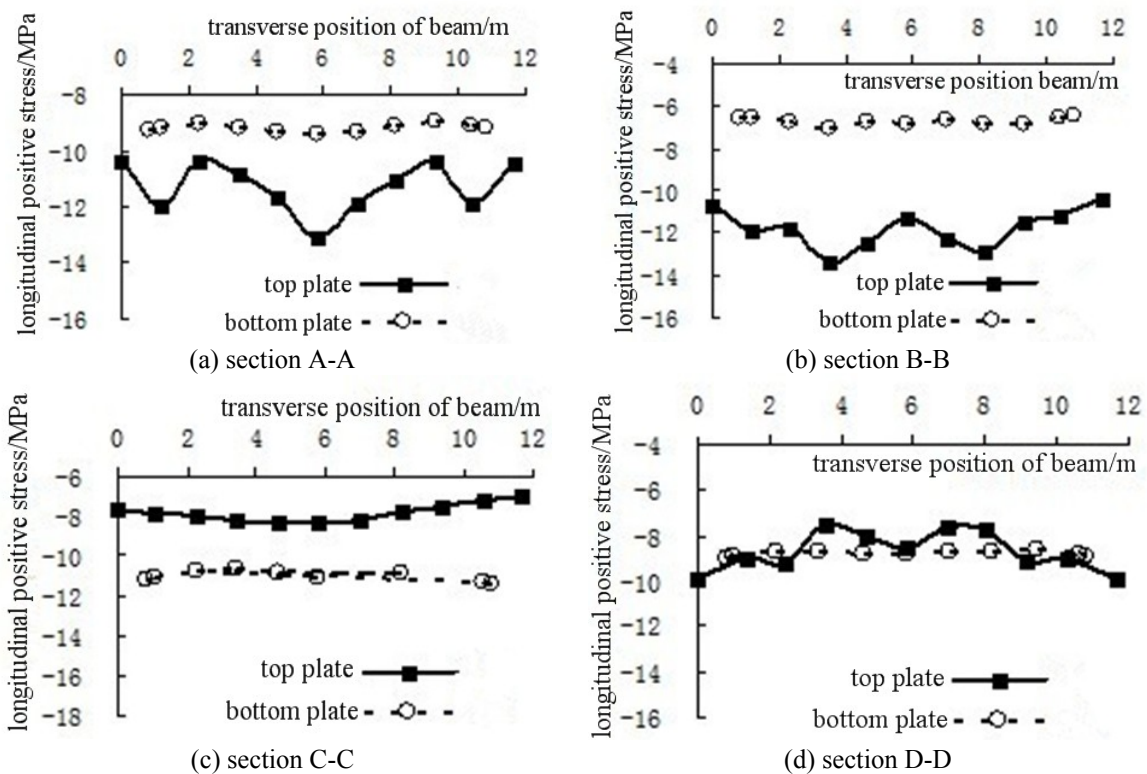


Fig. 10 Box beam longitudinal north stress transverse distribution of calculation section in half-bridge structure

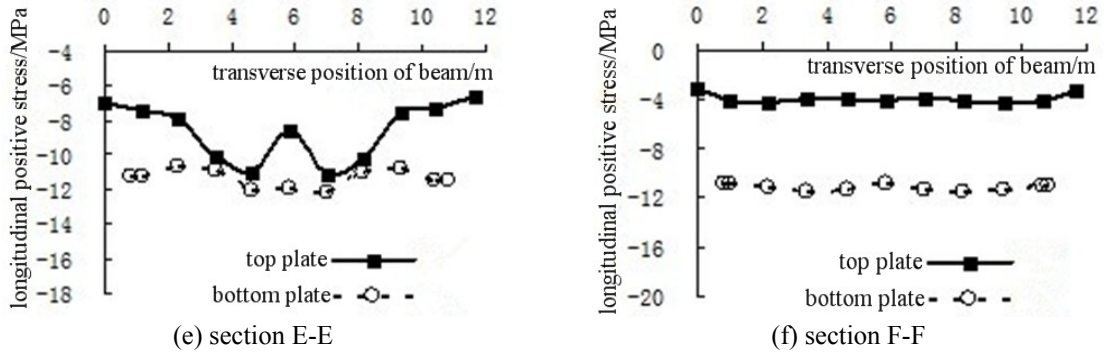


Fig. 10 Continued

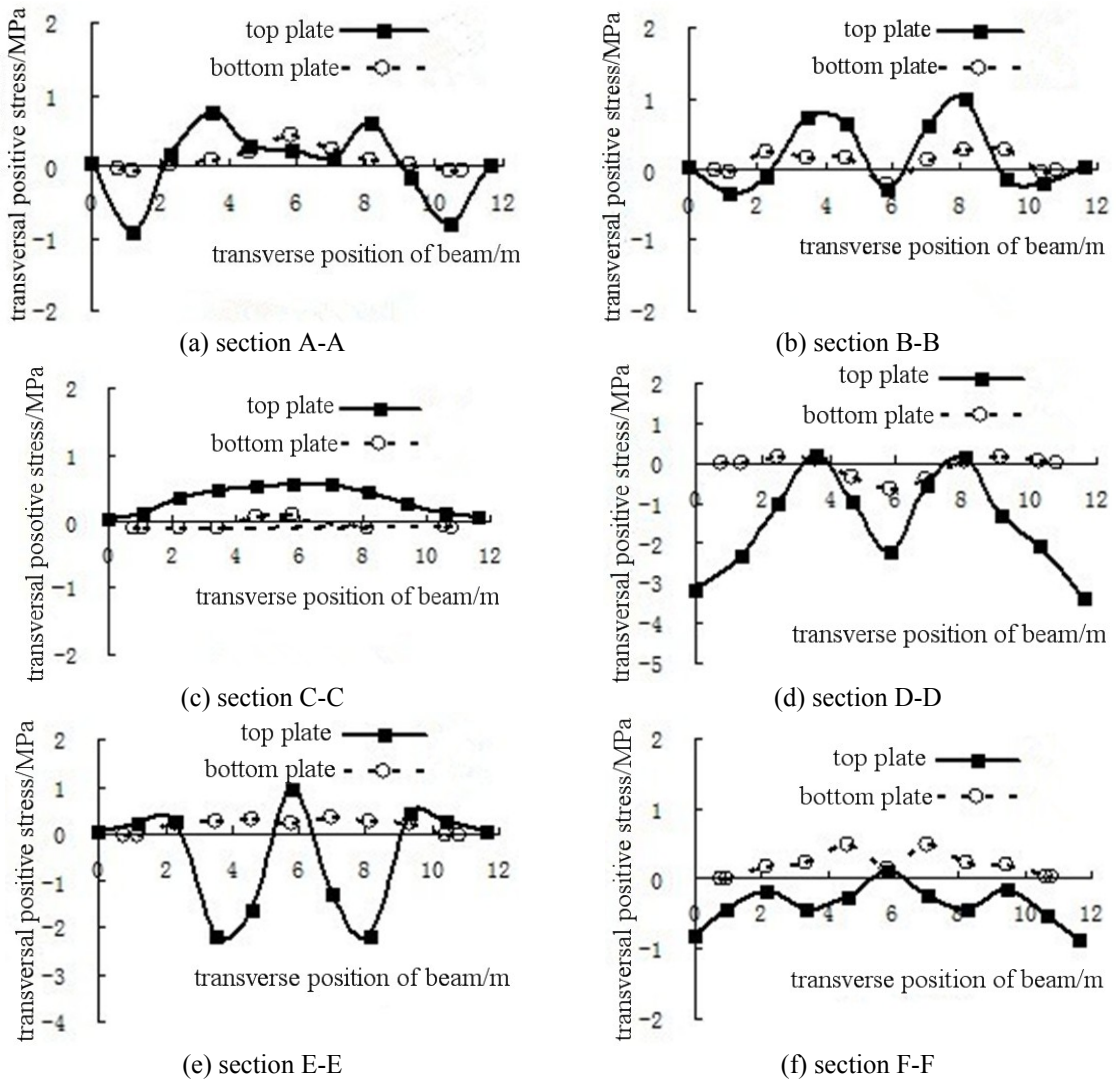


Fig. 11 Box beam transverse north stress transverse distribution of calculation section in half-bridge

5.3 Transversal bending positive stress of completed bridge's box girder

Fig. 11 shows transversal distribution of transversal bending positive stress in top and bottom plates of the six sections above-mentioned. The transversal bending compressive stress of whole bridge is small, within 1MPa, and the nonuniform extent of the distribution of transversal bending compressive stress in top plate is larger than that in the bottom plate. Although the top plate of box girder is in compressive status under dead loads and prestress effect, the transversal distribution of transversal bending positive stress is very nonuniform due to comprehensive effect of transverse prestress and longitudinal prestress in accordance with poisson ratio.

At the section of side span's mid-span: the maximum tensile stress at the point between two webs of top plate is 0.76MPa; in the mid web of top plate is 0.24MPa; at the section of V-shape pier and girder's junction at side span: the maximum tensile stress at the point between two webs of top plate is 0.99MPa, and the maximum compressive stress in top plate's mid web is -0.28MPa; at the section of V-shape pier and girder's junction at mid span: the maximum tensile stress at the point between two webs of top plate is 0.19MPa, and the maximum compressive stress in top plate's mid web is -2.18MPa; at the section of 1/4 mid span: the maximum compressive stress at the point between two webs of top plate is -2.19MPa, and the maximum tensile stress in bottom plate's mid web is 0.94MPa. The variation of the stress is acute, thus the results of plate analysis cannot reflect bridge's actual stress condition correctly.

The maximum transversal bending positive stress in the bottom plate of side span's mid-span is 0.43MPa, and 0.43MPa in the bottom plate of the junction of side span's V-shape pier and girder; the transversal bending positive stress in the bottom plate of mid span increases gradually from pier's top to mid-span; at the section of mid span's mid-span, the maximum tensile stress of top plate is 0.12MPa, and meanwhile 0.50MPa in bottom plate.

6. Conclusions

In this new type combined bridge, arch and girder take loads together. The structure's bending moment effect is mainly presented as mechanical characteristics of arch's compression and girder's tension. Hence, the advantage of arch and girder's mechanical characteristics are fully exerted. At the same time, the structure's vertical stiffness is large and its shape is light. The simulation calculation of whole bridge's construction process indicates that:

(1) The stress distribution of Xiaolan channel super large bridge's every section is in continuous variation, and with good regularity. The stress ratio of mid and side webs is larger in the side of span's sections, the value is about 1.20~1.96; the ratio in the sections of the main span is about 1.03~1.55; the element 0 and these three webs of the box girder on the top of the V-shape pier are stressed uniformly in accordance with structure forces.

(2) The construction envelope stress of the main girder is -18.60MPa~1.73MPa. The longitudinal positive stress of each section at construction stage can meet standard requirements, which indicates that longitudinal prestress can make the whole bridge in pressured state in longitudinal direction, and finally the expected purpose is achieved. Tensile stress almost does not appear in the construction process, in uniform variation and without mutation, indicating that the structure loading of element 0's box girder is reasonable. The stress value of each measuring point is within standard permissible value, which indicates that this bridge is safe in the construction process of erection of the continuous girder prior to that of the arches.

(3) The transversal distribution of longitudinal bending positive stress in section A-A, B-B, D-D and E-E's top plate is obviously nonuniform. Different from the predicted value given by elementary beam theory, the spatial effect and shear lag effect of prestress are obvious. The stress in the joint of flange and web is larger than that in the center at the sections of A-A and E-E, which is called positive shear lag phenomenon. And negative shear lag phenomenon appears at section B-B and D-D, because these sections are near cross strut at negative moment area. The restriction effect of pier and girder's consolidation point makes shear transfer from the junction of web and flange to plate's center lagged.

(4) The transversal bending compressive stress of whole bridge is small, within 1MPa, and the nonuniform extent of the distribution of transversal bending compressive stress in top plate is larger than that in the bottom plate. Although the top plate of box girder is in compressive status under dead loads and prestress effect, the transversal distribution of transversal bending positive stress is very nonuniform due to the comprehensive effect of transverse prestress and longitudinal prestress in accordance with poisson ratio.

Acknowledgements

The work described in this paper was partially supported by the National Natural Science Foundation of China (Grant Nos. 51108382), the Fundamental Research Funds for the Central Universities (Grant Nos. SWJTU12ZT20 and SWJTU11BR012).

References

- Nakamura, S.I. (2009), "Static analysis of cable-stayed bridge with CFT arch ribs", *Journal of Constructional Steel Research*, **65**(4), 776-783.
- Tao, Y. (2011), "Behaviour of a masonry arch bridge repaired using fibre-reinforced polymer composites", *Engineering Structures*, **33**(5), 1594-1606.
- Roeder, C.W. (2000), "Dynamic response and fatigue of steel tied-arch bridge", *Journal of Bridge Engineering*, **5**(1), 14-21.
- Ma, Y.S. (2011), "Creep effects on dynamic behavior of concrete filled steel tube arch bridge", *Structural Engineering and Mechanics*, **37**(3), 321-330.
- Haensel, J. (1998), "Composite bridge design: The reanimation of steel bridge construction", *Journal of Constructional Steel Research*, **46**, 54-55.
- Ribeiro, D. (2012), "Finite element model updating of a bowstring-arch railway bridge based on experimental modal parameters", *Engineering Structures*, **40**(7), 413-435.
- Altunisik, A.C. (2010), "Finite element model updating of an arch type steel laboratory bridge model using semi-rigid connection", *Steel and Composite Structures*, **10**(6), 541-561.
- Pan, S.S. (2011), "Reliability analysis for lateral stability of tongwamen bridge", *Steel and Composite Structures*, **11**(5), 423-434.
- Chen, J.F. (2002), "Load-bearing capacity of masonry arch bridges strengthened with fibre reinforced polymer composites", *Advances in Structural Engineering*, **5**(1), 37-44.
- Gou, H.G., Pu, Q.H. and Shi, Z. (2010), "Model test for the V-shape pier-girder joint of long-span V rigid frame composite arch bridge", *China Civil Engineering Journal*, **43**(3), 100-106.
- Wang, L. (2012), "Finite element simulation of residual stress of double-ceramic-layer La₂Zr₂O₇/8YSZ thermal barrier coatings using birth and death element technique", *Computational Materials Science*, **53**(1), 117-127.

- Roberts, I.A. (2009), "A three-dimensional finite element analysis of the temperature field during laser melting of metal powders in additive layer manufacturing", *International Journal of Machine Tools and Manufacture*, **49**(5), 916-923.
- Lee, D.H. (2009), "Analytical approach for the earthquake performance evaluation of repaired/retrofitted RC bridge piers using time-dependent element", *Nonlinear Dynamics*, **56**(4), 463-482.
- TB10002.3-2005(2005), "Code for Design on Reinforced and Prestressed Concrete Structure of Railway Bridge and Culvert", Beijing: China Railway Press.